Flat Plate Flutter in a Supersonic Flow Field

B. B. Ndebele
Council for Science and Industrial Research, 1 Meiring Road, Pretoria, South Africa

Corresponding Author's name: brightndebele@hotmail.com

Abstract
The interaction of a two-dimensional cantilevered elastic flat plate with a supersonic flow field was investigated numerically using StarCCM+. The plate was 0.4 m in length and inclined at 15° to the freestream at three Mach numbers (1.2, 1.35, and 1.45). The flat plate was assumed to be aluminium. Using StarCCM+, the inviscid Navier-Stokes equations were solved, and the fluid-structure interaction resolved. This way, the flow field around the plate and the plate deflection were calculated. The results indicated that at Mach 1.2, the plate exhibited a steady-state deflection, while at the other investigated Mach numbers, limit cycles were observed. The deformation of the plate caused a flow compression at the top, resulting in a weak shock at Mach 1.2 and strong shocks at 1.35 and 1.45. These findings provide insight into the dynamic response of the plate and the corresponding flow characteristics at different Mach numbers.

1 Introduction

When a supersonic flow field encounters an inclined rigid plane, it can create an attached or detached shock wave. The behaviour of this shock wave has been investigated by several researchers and is well understood. Consider, for example, Ben-dor's [1] exhaustive description of the state of the art of shock reflection phenomena. While understood, the specific details and behaviour of the shocks may vary depending on specific conditions of the flow, such as angle of incidence, fluid properties, as well as properties of the reflecting plane, such as thermal conductivity and wall porosity. Consider, for example, Cohen and Skews' [2] investigation of the influence of the reflecting plane's thermal conductivity on the shock reflection angle. In that investigation, they observed that surface thermal conductivity has non-negligible effects on shock reflection by showing that the Mach stem length during a Mach reflection is influenced by the surface thermal conductivity. Similarly, Skews [3, 4] investigated the influence of reflecting wall porosity and found that the angle of the reflected shock decreases with plate blockage. These cases help illustrate that the wall during a shock-wall interaction is an active participant.

Most investigations of shock reflection assume a rigid reflecting boundary. The interaction between an elastic boundary and a supersonic fluid has received some theoretical attention in the field of aeroelasticity regarding panel flutter [5–7]. Vedeneev [6] shows that a two-dimensional flat plate, constrained at both ends and in low supersonic flow ($1 < M < 2$), will experience so-called single mode flutter. In [7], Bondarev and Vedeneev investigated the influence of instabilities in the boundary layer on flat plate flutter. Relevant to this paper is the observation that in their investigation, the free stream is assumed to be a featureless and uniform flow. Plate deformation can induce disturbances that propagate and disrupt the free stream. Like in the present investigation, Currao et al. [8], investigated the flutter of a cantilevered plate; but unlike this paper, they considered hypersonic flow ($M = 5.8$) where a shock is incident on a flat plate to interfere with the boundary layer. In general, they observe limit-cycle oscillations and laminar turbulent boundary layer transitions.

This investigation seeks to investigate the stability of a flexible plate at an angle of attack in an otherwise steady supersonic flow field. The flow field and its features are then described. It

is then posited that there exists a threshold Mach number that delimits the case when the plate flutters indefinitely and when the plate returns to its static deformation.

2 Methodology

StarCCM+ was used to conduct Computation Fluid Dynamics (CFD) simulations and to analyse the interaction of the fluid structure with the flexible plate. The solver setup; computational domain; and grid are described in Section 2.1. Grid independence is described in Section 2.2.

2.1 CFD Setup

Figure 1 shows a schematic of the two-dimensional simulation domain. The domain was circular with a radius (Z) of 10 m and the left edge of the plate was 5 m (X) from the boundary of the incoming flow. The left-hand side of the plate was fixed. Plates of width 0.01 m and length (Y) 0.4 m were investigated.

In the simulations, a hexahedral mesh was used. The flat plate was made up of hex cells with a uniform size of 5×10^{-4} m. The fluid domain in the vicinity of the plate was set to a uniform cell size of 1×10^{-4} m. Note that the mesh deforms as the plate deflects, which can affect the quality of the mesh. For this application, this cell size was chosen because it was found to preserve adequate cell quality. The volume growth rate was set at 1.05 so that the volume mesh cell size grew to a maximum of 0.7 m at the far-field boundary. The typical cell count for these specifications was 208 000 cells.

The fluid, assumed to be air, was modelled as an inviscid ideal gas, whereas the plate was modelled as an aluminium material with isotropic properties. The density, Poisson ratio, Young's modulus of aluminium was set as 2702 kg.m^{-3}, 0.33, and 6.8×10^{10} Pa, respectively. These properties correspond to Aluminium 1350. Furthermore, it was assumed that the deformation of the plate was linear. The timestep was set to 5×10^{-4} seconds and each inner iteration was set to complete in thirty iterations. The fluid flow field was initially decoupled from the structure for the first 0.02 seconds of the simulation, and the full fluid-structure coupling was set to occur after 0.025 seconds. Between these two intervals, the fluid forces on the structure were increased linearly. Structural dynamics was modelled using Equation (1) where **M**, **C**, and **K** represent the mass matrix of the structure, the damping matrix, and the stiffness matrix, respectively.

Structural physical damping (**C)** was introduced using the Rayleigh damping model formulated as equation (1), where **K** and **M** are the stiffness and mass matrices of the structure, respectively. The term on the right-hand side (f^{ext}) accounts for all external forces that are imposed on the structure. Unlike the mass and stiffness matrices that are known, damping is difficult to estimate due to its complexity. Therefore, the Rayleigh model was used here to approximate structural damping. The model (Equation 2) assumes that the structural damping is a linear combination of the mass and stiffness matrices with parameters τ_k and f_M. The two parameters are structure dependent and were set to 0.0055 Hz and 2×10^{-7} respectively.

$$\boldsymbol{M\ddot{u}}(t) + \boldsymbol{C\dot{u}}(t) + \boldsymbol{Ku}(t) = \boldsymbol{f}^{ext} \tag{1}$$

$$\boldsymbol{C} = \tau_k \boldsymbol{K} + f_M \boldsymbol{M} \tag{2}$$

The fluid flow was modelled using the Navier-Stokes equation (3), where ρ, $\boldsymbol{v}$, E, and σ represent the fluids density, velocity, energy, and stress respectively. Equations (2) and (3) were both implemented in StarCCM+.

$$\frac{\partial \boldsymbol{U}}{\partial t} + \Delta \cdot \boldsymbol{Q} = \boldsymbol{R} \tag{3}$$

$$U = \begin{pmatrix} \rho \\ \rho \boldsymbol{v} \\ \rho E \end{pmatrix}, Q = \begin{pmatrix} \rho \boldsymbol{v} \\ \rho \boldsymbol{v}\boldsymbol{v} \\ \rho E \boldsymbol{v} \end{pmatrix}, \text{ and } R = \begin{pmatrix} 0 \\ \Delta \cdot \boldsymbol{\sigma} + \boldsymbol{f}_{ext} \\ f_{ext} \cdot \boldsymbol{v} + \Delta \cdot (\boldsymbol{v} \cdot \boldsymbol{\sigma}) \end{pmatrix}$$

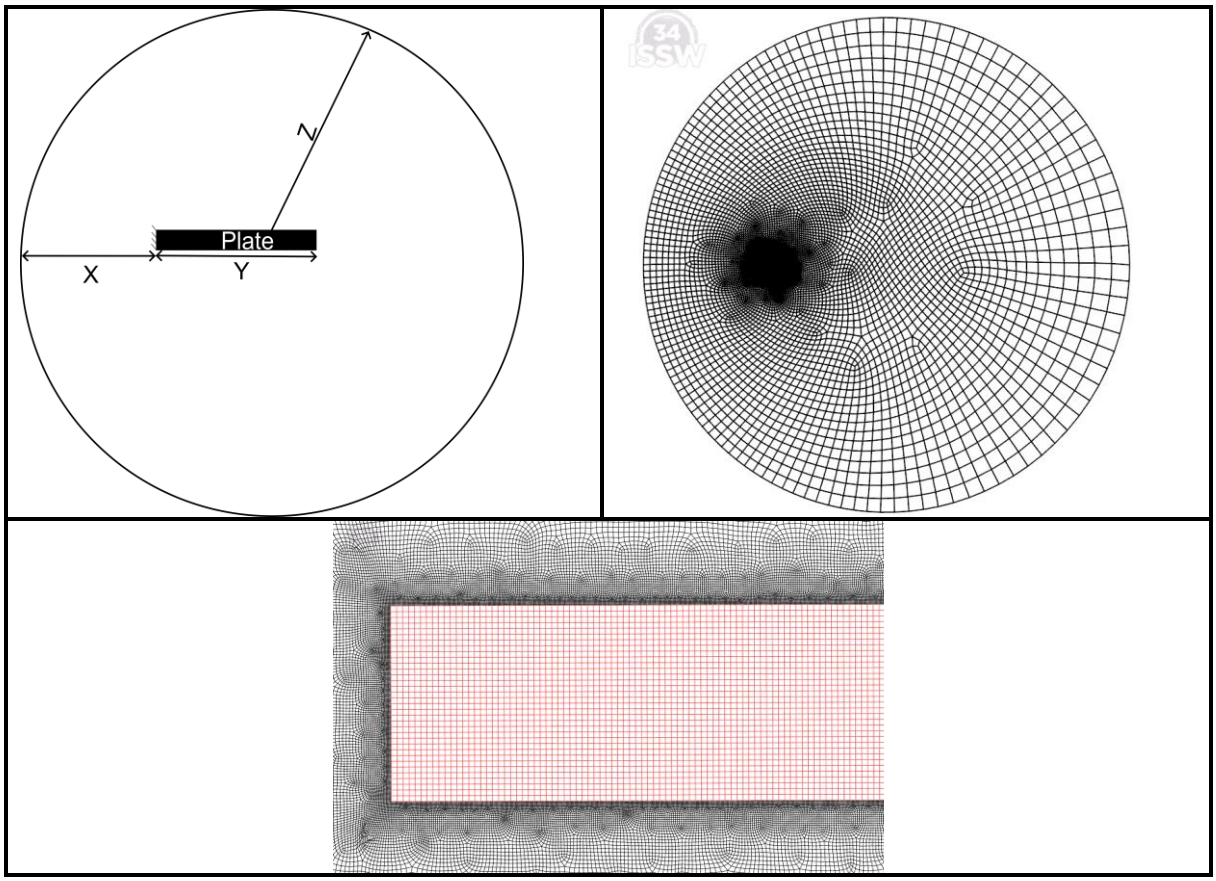

Figure 1: Computational domain used to perform CFD analysis. The images on the left and bottom show the typical hex mesh that was used.

2.2 Grid Independence

Grid independence studies were conducted as described by Roache [9], which led to the calculation of the so-called grid convergence index (GCI). The GCI represents the percentage error in the measured quantity attributable to the grid. The mesh independence study was carried out using steady-state converged solutions and the GCI calculated based on plate drag and lift coefficients and plate maximum normalised deflection. The GCI is calculated as shown in Equation (4) and the deflection normalisation is shown in Equation (5). In (4), ϵ is the difference between the monitored quantities calculated using two different grids (coarse and fine); r is the refinement factor between the two grids; and p is the order of the CFD algorithm. The parameter Δ_{min} in Table 1 represents the smallest element in the grid. Thus, the grid of Case 0 was the coarsest and formed the basis for the finer cases (Case 1 and 2). Each subsequent case was 1.6 smaller than the next coarse case. The calculated GCI are shown in Table 1. The GCIs for Cases 1 and 2 are calculated relative to Case 0. The GCIs in Table 1 represent the grid error for grids 1 and 2. GCI_D and GCI_δ for Case 2 are sufficiently small and hence that the grid was used in all simulations.

$$GCI = \frac{\epsilon}{1 - r^p} \tag{4}$$

$$\delta = \frac{\text{Plate Deflection}}{\text{Plate Thickness}} \tag{5}$$

Table 1: Grid Convergence Indices for three grid refinement levels calculated using plate drag, lift, and deflection.

Case	#Cells	D	L	δ	Δ_{min} (mm)	GCI_D	GCI_L	GCI_δ
0	195264	1.78	-0.45	0.0017	0.185	-	-	-
1	392665	1.77	-0.36	0.0013	0.115	0.0162	0.147	6×10^{-4}
2	854501	1.80	-0.36	0.0014	0.072	0.0211	0.095	3×10^{-4}

2.3 Cases Investigated

With the grid established, the plate's stability at Mach numbers 1.2, 1.35, and 1.45 was investigated with the angle of attack set to $15°$. It was expected that at some angle of attack (in this instance $15°$), an asymmetric detached shock would form in front of the plate, causing a pressure difference between the top and bottom surfaces of the plate and hence the plate deformation. Plate deformation would then influence the near flow field (e.g., the wake and shock location), potentially causing sustained plate oscillations. The results and discussion of the simulations are presented in Section 3.

3 Results and Discussion

The fluid and the structure considered in this investigation form a dynamic system in which there is an exchange of energy between the fluid and the structure. Such systems can be stable as illustrated by the Mach 1.2 case where oscillations are observed to die out to a steady deflection. Alternatively, the systems can exhibit limit cycle oscillations such as Mach 1.35 and 1.45. In a limit cycle oscillation, the system is characterised by closed-loop trajectories in a phase space such as a space defined by tip deflection and normal force [10]. Between the stable behaviour and the limit-cycle oscillation must exist a bifurcation point, parameterised by Mach number, marking the switch in behaviour.

The time histories of the tip deflection for each Mach number are shown in Figure 2 on the left. In all three cases, the plate oscillates about some mean point; however, at Mach 1.2 the amplitude of the oscillation decreases monotonically, while at Mach 1.35 and 1.45 the amplitude increases to a steady value. Although not shown, the Mach 1.2 case approaches a steady deflection, and the other two cases approach limit-cycle oscillations. A Fourier analysis of the tip signals reveals that the tips oscillate at a frequency of 69.2 Hz and 72.5 Hz for Mach numbers 1.2 and 1.35, and Mach 1.45 respectively which is indicative of single-mode oscillation. This is like Vedeneev's findings [6] of single-mode flutter.

Figure 3 to Figure *5* show Mach number contours around the plate over one period of the plate oscillation. The figures show that a detached shock stands in front of the plate, and as will be shown, the standoff distance of the shock oscillates about a mean position at the same frequency as the deflection frequency of the tip. Recall that the plate is at a $15°$ angle of attack, so that the initial pressure difference between the top and bottom surfaces causes the plate's initial deflection, which results in internal stresses within the plate that act to straighten the plate. The interplay between pressure imbalance and the plate's internal stresses is one of the reasons for the observed oscillation.

As the plate deforms, its curvature alternates between concave and convex as shown in the Mach number contours below. Consider, for example, Figure 3b, 5e, and 6e, where the upper surface of the plate is convex and the lower surface concave: in all three cases, a secondary attached shock is observed on the top surface, while an expansion fan is seen at the bottom. These are not permanent features but depend on the deflection of the plate. Therefore, to describe the evolution of the flow field over one oscillation cycle, consider Figure 5, which has clearer features. An asymmetric bow shock is present in all frames. At the fixed edge stands an expansion fan followed by a weak curved shock (S_A). There appears to be an interaction between S_A and the rear shock S_B as highlighted in (a). Note that this interaction is not present when the plate returns to the same position in frame (c). In frame (b), S_A has been significantly weakened as the plate adopts a convex orientation. As the plate transitions towards a concave orientation, the accelerated flow after the expansion fan is compressed to reform S_A, which in turn interacts with S_B. The effect of the interaction between S_A and S_B on the wake of the plate can be seen in Figure 6. In Figure 6a, S_A has weakened; in Figure 6b, the interaction between S_A and S_B is evident, showing the reflected shock (R), transmitted shock (T), and shear layer (S). The reflected shock perturbs the orientation of the plate wake, resulting in a regular pattern. Indeed, by placing a pressure probe in the wake, the wake was observed to oscillate at the same frequency as the plate. On the convex bottom surface, the expansion wave (EW_B) interacts with the bow shock and changes the curvature of the shock. This description can be extended to other Mach numbers.

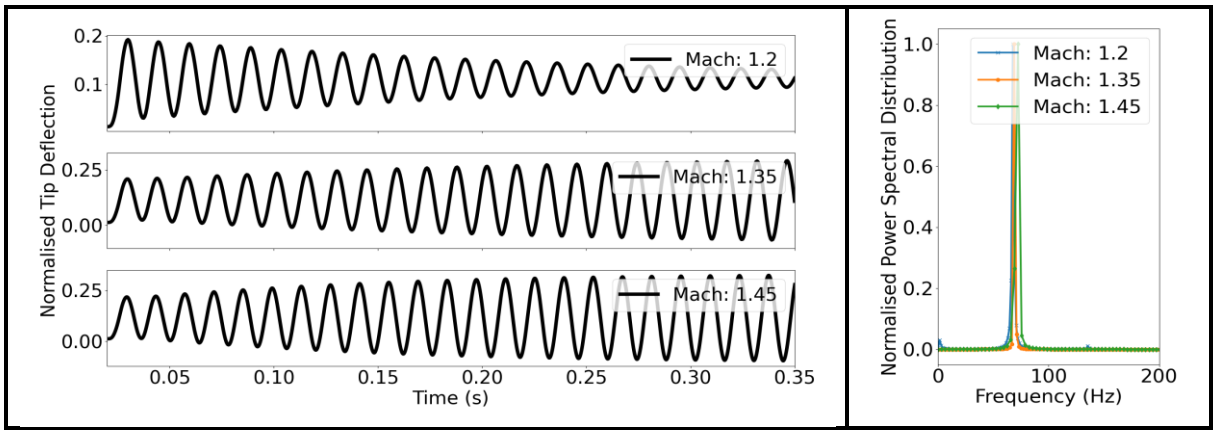

Figure 2: A time history of normalised plate deflections at Mach 1.2, 1.35, and 1.45. Plate deflections are normalised by dividing the deflections by plate length.

Figure 7 shows the phase plots that describe the behaviour of the plate. From the figure, at Mach 1.2, the plate tends towards a steady-state behaviour also seen in Figure 2. This can be explained by considering the flow field shown in Figure 3. At this Mach number, the initial concave deformation of the plate results in a weak shock wave at the top of the plate (Figure 3b); compare this with Figure 4e and 6e, where the shocks are stronger. As a result, the plate deformation is quickly damped in contrast to the Mach 1.35 and 1.45 cases, each of which approaches limit-cycle oscillations. Figure 7b, c, and d show a hysteresis effect that is indicative of a phase difference between the plotted quantities. From Figure 7b, we see that the maximum and minimum shock stand-off distances do not occur at the maximum or minimum tip deflections; a similar deduction can be made about the normal force experienced by the plate (Figure 7c). Since the phase plot curves seem to form a closed curve, it can be concluded that the shock stand-off, normal force, and normal stress fluctuate at the same frequency as the tip oscillation.

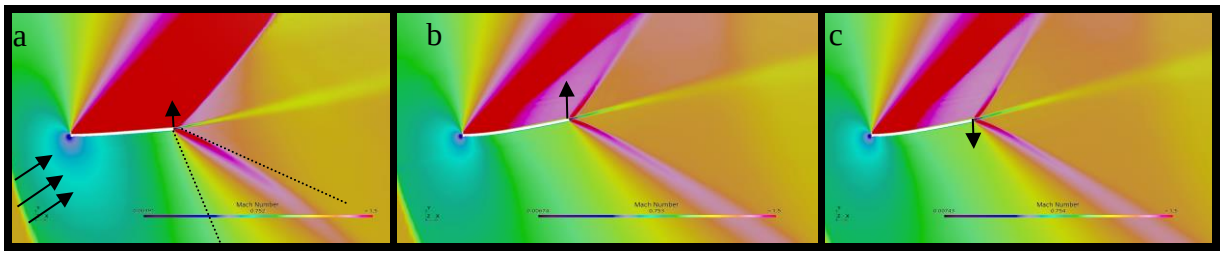

Figure 3: Mach number contours around a flexible flat plate at Mach 1.2 over one complete oscillation.

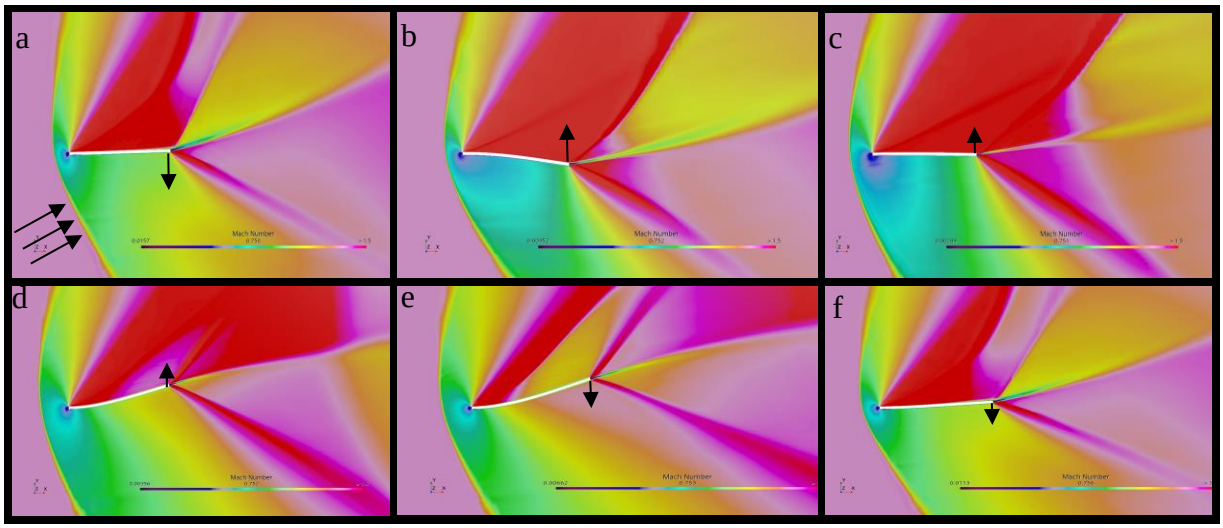

Figure 4: Mach number contours around a flexible flat plate at Mach 1.375 over one complete limit cycle oscillation.

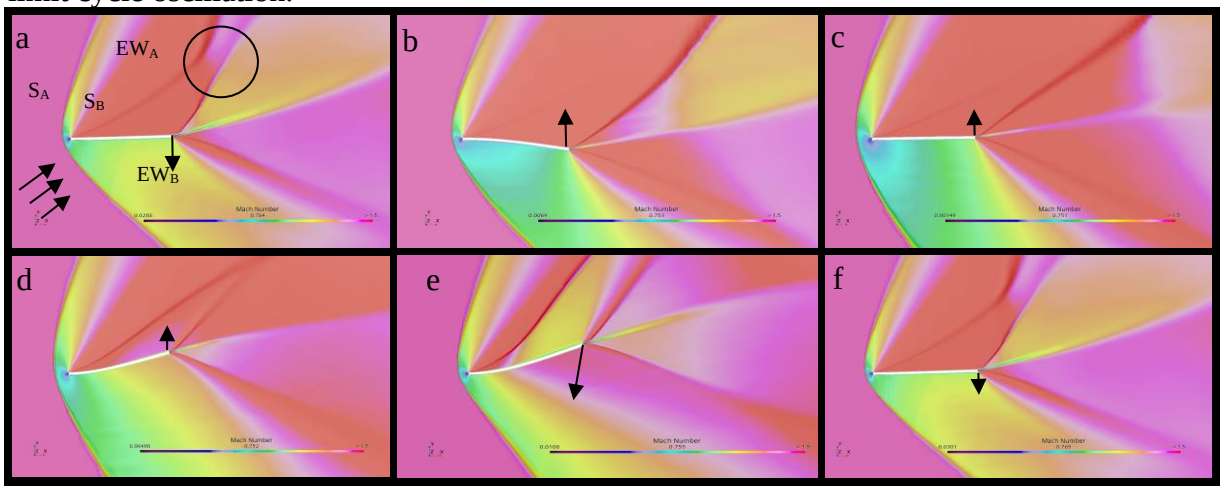

Figure 5: Mach number contours around a flexible flat plate at Mach 1.45 over one complete limit cycle oscillation.

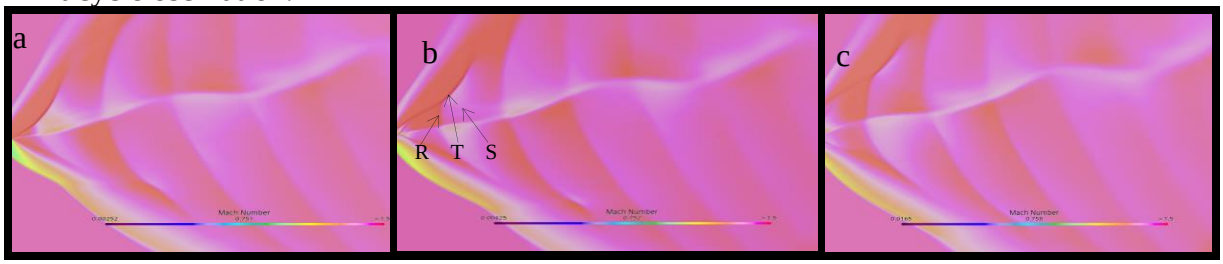

Figure 6: Detached shock and wake distortion.

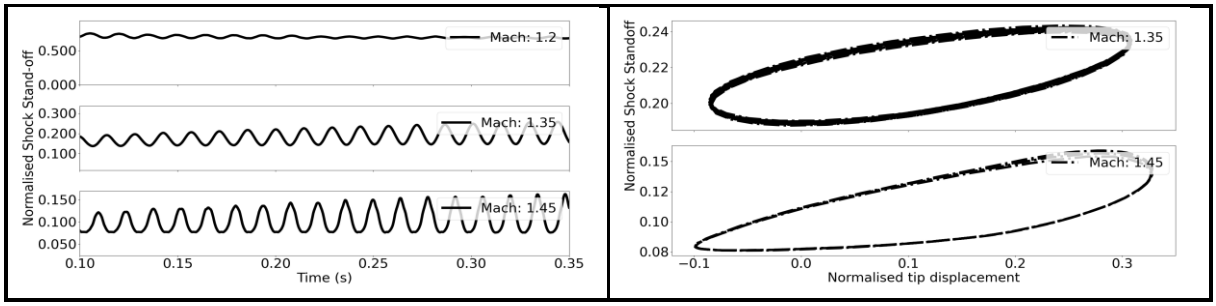

a.) Shock stand-off distance variation. b.) Stand-off/plate deflection phase plot.

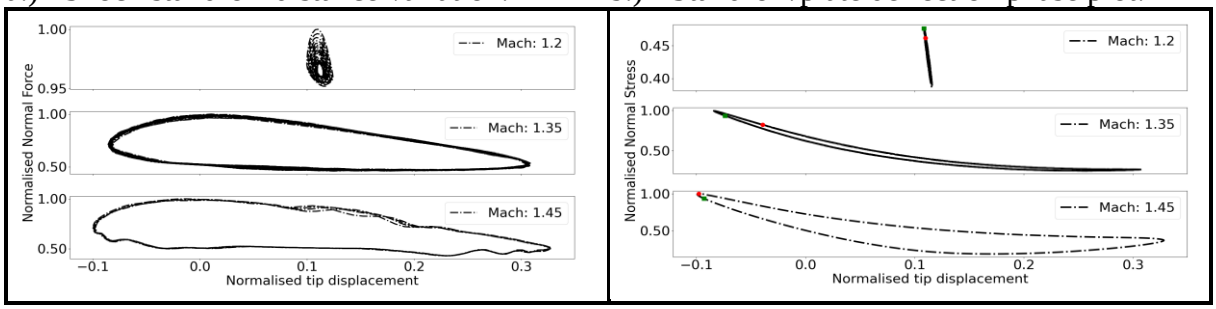

c.) Force and tip displacement phase plot. d.) Stress and tip displacement phase plot.

Figure 7: Flat-plate quantitative behaviour at three Mach numbers. The standoff distance and plate deflection were normalised by dividing by plate length, while forces and stresses were normalised by their respective maximums.

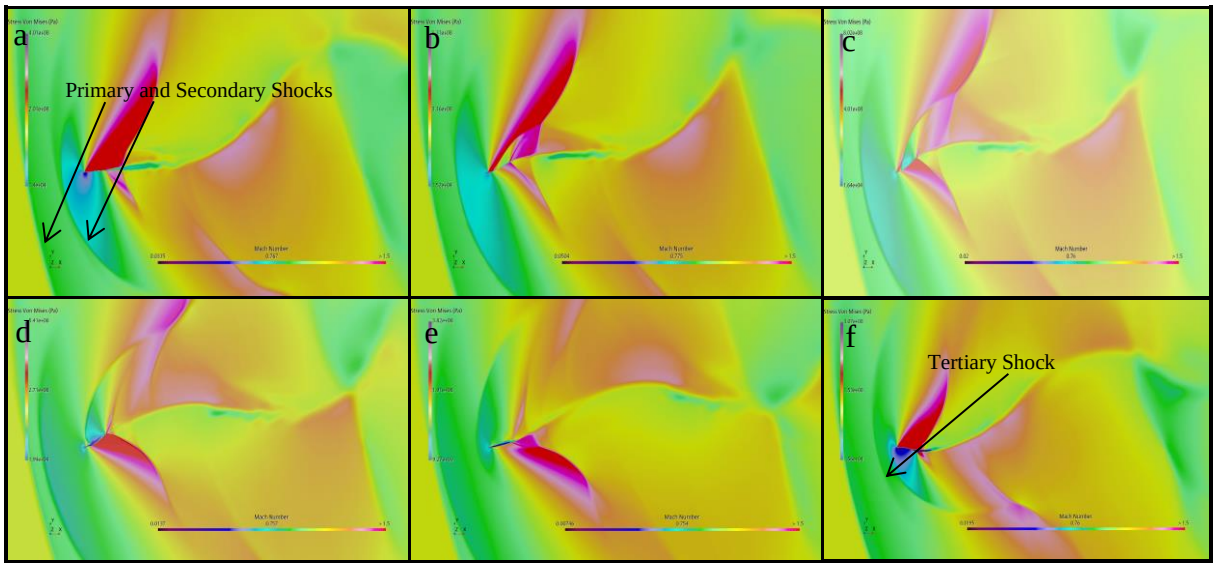

Figure 8: Mach number contours around a 0.8 m long flat plate at Mach 1.1 over one complete oscillation

Now, consider a longer plate (0.8 m) at Mach 1.1 as shown in 8. Considering that the 0.4 m long plate oscillations were damped at Mach 1.2, it was surprising that the longer plate exhibited limit cycle oscillations at an even lower Mach number (Figure 9). As the plate was longer, it also had a larger maximum tip displacement and surface area to accelerate the flow. We saw in Figure 5a that as the tip curves upwards, the flow on the top side accelerates to form a shock (S_A); on a longer plate, the combination of acceleration and larger tip deflection eventually results in a secondary detached shock (Figure 8a). S_A can be seen detaching in frame (d). The secondary shock is shed from the plate and propagates upstream towards the primary shock.

Figure 9b shows a kink in the phase plot, indicative of a sudden change in the force distribution on the plate. This is related to the moment the secondary shock is absorbed from the top plate. A third shock (Figure 8f) forms when the plate deflects downward. This shock eventually swept downstream.

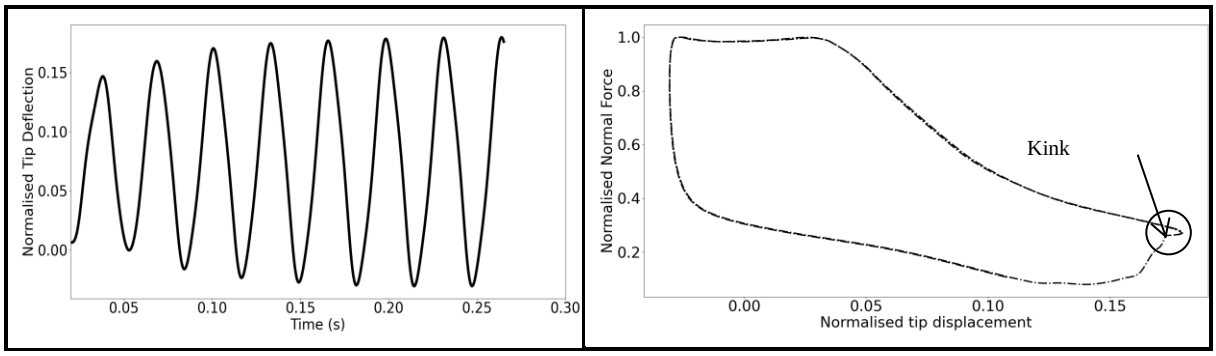

Figure 9: A time history of normalised plate deflection at Mach 1.1 for a 0.8 m long plate [left] and normal force-tip deflection polar [right]

From the above, we can see that whether a plate of fixed length oscillates or is stable is influenced by the flow Mach number. A brute-force approach was implemented to find the threshold Mach number where a 0.4 m long plate switches behaviour. Given two Mach numbers in which the plate oscillates and is stable, a third simulation was performed at the midpoint Mach number. This procedure provides an interval within which this threshold should exist. Repeating this procedure several times can arbitrarily narrow the interval. Therefore, having identified an initial interval (1.2, 1.35) the above bisection procedure was executed to narrow the interval to (1.25625, 1.275).

4 Conclusions

The flutter of a flat plate at a 15° angle of attack was investigated. The investigation showed that:

- At Mach 1.2 the flat plate tends towards a steady-state deformation, while limit cycle oscillations are observed at Mach 1.35 and 1.45.
- There must be a threshold Mach number where the transition from steady-state behaviour to limit cycle oscillation occurs. This threshold value was determined to be between Mach 1.25625 and 1.275 exclusively.
- Plate deformation compresses the supersonic flow at the top of the plate, leading to the formation of a dynamic shock wave.
- The bow shock in front of the flat plate oscillates at the same frequency as the flat plate.
- As the bow shock oscillates and the plate deforms, the expansion waves at the trailing edge of the plate deform the shock profile.

This investigation did not account for the thermal fluctuations of the plates as the plate flexes. This heating contributes to structural damping by converting some of the energy imposed on the structure into heat.

References

[1] Ben-Dor, G., *Shock Wave Reflection Phenomena*, 2nd ed. New York, NY: Springer New York, 1992. doi: 10.1007/978-1-4757-4279-4.

[2] Cohen, A., and Skews, B. W., “Surface conductivity effects during shock wave reflection off curved surfaces,” *Exp Therm Fluid Sci*, vol. 124, p. 110353, Jun. 2021, doi: 10.1016/J.EXPTHERMFLUSCI.2021.110353.
[3] Skews, B., “Shock wave interaction with porous plates,” *Exp Fluids*, vol. 39, no. 5, pp. 875–884, 2005, doi: 10.1007/s00348-005-0023-7.
[4] Skews, B. W., “Oblique reflection of shock waves from rigid porous materials,” *Shock Waves*, vol. 4, no. 3, pp. 145–154, 1994, doi: 10.1007/BF01417430.
[5] Mei, C., Abdel-Motagaly, K., and Chen, R., “Review of Nonlinear Panel Flutter at Supersonic and Hypersonic Speeds,” *Appl Mech Rev*, vol. 52, no. 10, pp. 321–332, Oct. 1999, doi: 10.1115/1.3098919.
[6] Vedeneev, V. V., “Limit oscillatory cycles in the single mode flutter of a plate,” *Journal of Applied Mathematics and Mechanics*, vol. 77, no. 3, pp. 257–267, 2013, doi: https://doi.org/10.1016/j.jappmathmech.2013.09.001.
[7] Bondarev, V., and Vedeneev, V., “Short-wave instability of an elastic plate in supersonic flow in the presence of the boundary layer,” *J Fluid Mech*, vol. 802, pp. 528–552, 2016, doi: DOI: 10.1017/jfm.2016.482.
[8] Currao, G. M. D., Neely, A. J., Kennell, C. M., Gai, S. L., and Buttsworth, D. R., “Hypersonic Fluid–Structure Interaction on a Cantilevered Plate with Shock Impingement,” *AIAA Journal*, vol. 57, no. 11, pp. 4819–4834, Jul. 2019, doi: 10.2514/1.J058375.
[9] Roache, P. J., “Quantification of Uncertainty in Computational Fluid Dynamics,” *Annu Rev Fluid Mech*, vol. 29, no. 1, pp. 123–160, Jan. 1997, doi: 10.1146/annurev.fluid.29.1.123.
[10] Strogatz, S. H., “Nonlinear Dynamics and Chaos,” Boca Raton: *CRC Press*, 2015